iScience

CellPress
OPEN ACCESS

Article

Photoinduced chlorophyll charge transfer state identified in the light-harvesting complex II from a marine green alga *Bryopsis corticulans*

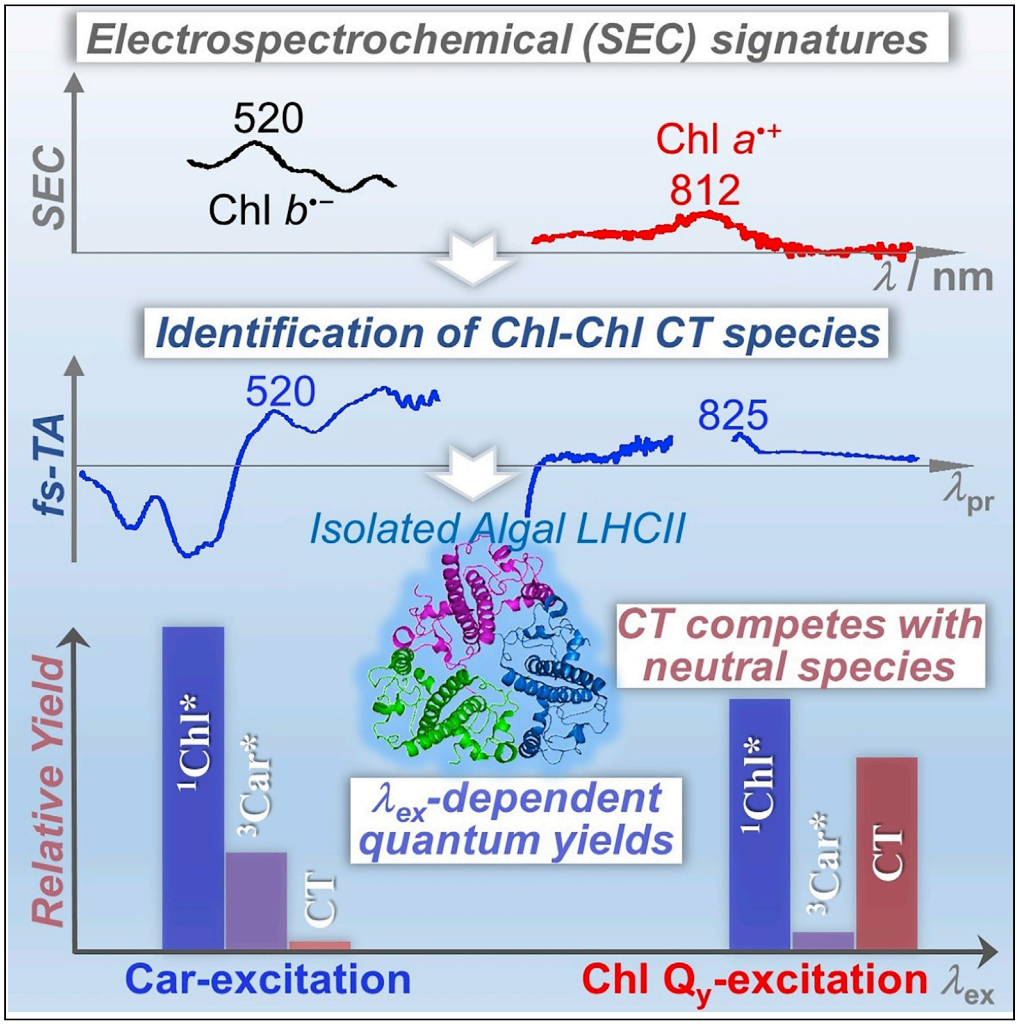

Dan-Hong Li, Wenda Wang, Cuicui Zhou, ..., Jian-Ren Shen, Tingyun Kuang, Jian-Ping Zhang

kuangty@ibcas.ac.cn (T.K.)
jpzhang@ruc.edu.cn (J.-P.Z.)

Highlights

Ultrafast spectroscopy of a carbonyl Car containing LHCII in trimeric form

Ultrafast photogeneration of Chl *a* and Chl *b* radical ions upon Chl Q_y excitation

Chl charge transfer species formation is competitive with ^{1}Chl* relaxation

Carbonyl Car-to-Chl singlet excitation energy transfer in picosecond timescale

Li et al., iScience *26*, 105761
January 20, 2023
https://doi.org/10.1016/j.isci.2022.105761

iScience

CellPress
OPEN ACCESS

Article

Photoinduced chlorophyll charge transfer state identified in the light-harvesting complex II from a marine green alga *Bryopsis corticulans*

Dan-Hong Li,[1,4] Wenda Wang,[2] Cuicui Zhou,[2] Yan Zhang,[1] Songhao Zhao,[2] Yi-Ming Zhou,[1] Rong-Yao Gao,[1] Hai-Dan Yao,[1] Li-Min Fu,[1] Peng Wang,[1] Jian-Ren Shen,[2,3] Tingyun Kuang,[2,*] and Jian-Ping Zhang[1,5,*]

SUMMARY

The light-harvesting complex II of *Bryopsis corticulans* (*B*-LHCII), a green alga, differs from that of spinach (*S*-LHCII) in chlorophyll (Chl) and carotenoid (Car) compositions. We investigated ultrafast excitation dynamics of *B*-LHCII with visible-to-near infrared time-resolved absorption spectroscopy. Absolute fluorescence quantum yield (Φ_{FL}) of LHCII and spectroelectrochemical (SEC) spectra of Chl *a* and *b* were measured to assist the spectral analysis. Red-light excitation at Chl Q_y-band, but not Car-band, induced transient features resembling the characteristic SEC spectra of Chl $a^{\cdot+}$ and Chl $b^{\cdot-}$, indicating ultrafast photogeneration of Chl-Chl charge transfer (CT) species; Φ_{FL} and ^{3}Car* declined whereas CT species increased upon prolonging excitation wavelength, showing positive correlation of ^{1}Chl* deactivation with Chl-Chl CT formation. Moreover, ultrafast Chl *b*-to-Chl *a* and Car-to-Chl singlet excitation transfer were illustrated. The red-light induction of Chl-Chl CT species, as also observed for *S*-LHCII, is considered a general occurrence for LHCIIs in light-harvesting form.

INTRODUCTION

In oxygenic photosynthesis, the major light-harvesting complex of photosystem II (LHCII) binds chlorophylls (Chls) accounting for about half of the total pigments of thylakoid membranes, and plays crucial roles in both light harvesting and photoprotection.[1,2] The LHCII antenna captures sunlight and transfers the electronic excitation energy to the photosystem II (PSII) reaction center to drive the primary electrochemical reactions therein. However, the excessive electronic excitation resulting from overabundant light illumination must be dissipated safely, as it will otherwise impose photoinhibition to PSII and irreversible oxidative damage to the photosynthetic proteins. In this respect, LHCII provides important photoprotection by converting the excessive Chl singlet excitation (^{1}Chl*) into harmless heat before sending it to the reaction center, a mechanism often referred to as energy-dependent quenching (qE).[3–5] Carotenoids (Cars) in photosynthesis is known to be an accessory light harvester, as well as a structural stabilizer, photoprotector, and scavenger of reactive oxygen species (ROS).[6–9] In addition, the Cars bound to LHCII are involved in the qE process via incoherent[5,10–13] or coherent[14,15] Chl-to-Car excitation energy transfer (EET), or via Car-Chl charge transfer (CT) interaction,[16,17] an issue which has attracted considerable research efforts but still remains unresolved. Indubitably, the mechanistic understandings have benefited from the advances in unraveling the structural details of LHCII and PSII-LHCII supercomplexes of higher plants and a green alga.[18–22] However, a variety of green algae are present, and some of them have different pigment compositions and ratios from that of the model green alga *Chlamydomonas reinhardtii* from which the structure of PSII-LHCII is solved. A parallel understanding of green algal photosynthesis has been left behind owing to the shortage of structural information on the relevant pigment-protein complexes.

Bryopsis corticulans is a siphonaceous green alga living in nearshore intertidal zones under changing light conditions. Biochemical and spectroscopic analyses showed that *B. corticulans* LHCII (*B*-LHCII) is homologous to spinach LHCII (*S*-LHCII) in both protein sequences and pigment binding sites.[23,24] Similar to *S*-LHCII, *B*-LHCII is in trimeric form, however, each Lhcb subunit binds 6 Chls *a*, 8 Chls *b*, 1 Neoxanthin (Neo), and 3 keto-Cars including siphonein (Spn) and siphonaxanthin (Spx). Such pigment composition means, with reference to *S*-LHCII, 2 Chls *a* out of the total 14 Chls are replaced by Chls *b*, and none of

[1]Key Laboratory of Advanced Light Conversion Materials and Biophotonics, Department of Chemistry, Renmin University of China, Beijing 100872, China

[2]Key Laboratory of Photobiology, Institute of Botany, Chinese Academy of Sciences, Beijing 100093, China

[3]Research Institute for Interdisciplinary Science, and Graduate School of Natural Science and Technology, Okayama University, Okayama 700-8530, Japan

[4]School of Biological and Behavioural Sciences, Queen Mary University of London, Mile End Road, London E1 4NS, UK

[5]Lead contact

*Correspondence: kuangty@ibcas.ac.cn (T.K.), jpzhang@ruc.edu.cn (J.-P.Z.)

https://doi.org/10.1016/j.isci.2022.105761

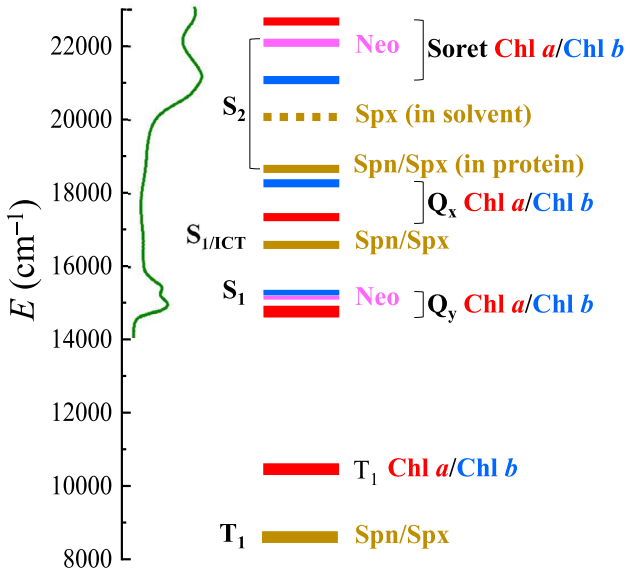

Scheme 1. Excited-state energy levels of Cars and Chls of *B*-LHCII

Excited-state energy levels of neoxanthin (Neo) and siphonaxanthin (Spx) are taken from ref. [27] and ref. [28]. The S_1 state energy of Siphonein (Spn) is assumed to be the same as that of Spx. Subscripts 1/ICT represent the mixing of the S_1 state with the intramolecular charge transfer (ICT) state.

the xanthophyll-cycle Cars such as violaxanthin and zeaxanthin present in *B*-LHCII. In addition, Spn and Spx in *B*-LHCII are most likely bound to the Lut620 and Lut621 sites, respectively, as in the case of *S*-LHCII.[23] It had been shown that both Spn and Spx can efficiently quench ^{3}Chl* and that the Chl fluorescence of *B*-LHCII is considerably less quenched in comparison with *S*-LHCII.[25] In addition, ultrafast spectroscopic studies revealed that *B*-LHCII compared to *S*-LHCII shows slower excitation equilibration (about 10 ps), which is likely due to the weaker coupling among Chls.[24] It is established for higher plants that photosynthetic organisms are protected against the high-light induced oxidative stress by the non-photochemical quenching (NPQ) mechanism. In this token, however, it is interesting that for *B. corticulans* the NPQ activity is independent of ΔpH, xanthophyll-cycle pigments, and allosteric induction proteins (PsbS and LhcSR), implying an NPQ behavior distinctly different from higher plants.[26]

As depicted in Scheme 1, the lowest lying singlet-excited states of Spn and Spx, $S_1(2A_g^-)$,[27,28] lie energetically above the Q_y states of Chl *a* and Chl *b*. Therefore, this pair of keto-Cars can serve as the accessary light harvester transferring excitation energy to Chls, rather than as the quencher of ^{1}Chl* via Chl-to-Car EET as the pair of lutein does in *S*-LHCII. Here, a question arises as to whether *B*-LHCII bears the qE-dependent photoprotection mechanism as plant LHCII does and, if so, what kind of molecular mechanism is in operation. In addition, in spite of a subtle variation in molecular structures, Chl *b* differs from Chl *a* in excited-state dynamics and energetics such as nonradiative relaxation properties, fluorescence lifetimes, triplet yields, as well as redox potentials.[29–31] Therefore, the unique keto-Cars and the relatively high Chl *b*/*a* ratio may endow *B*-LHCII with peculiar light-harvesting and photoprotection properties.

To explore the light-harvesting and photoprotection mechanisms of *B*-LHCII, we employed femtosecond time-resolved absorption (*fs*-TA) spectroscopy, which is rather sensitive to the pigment interactions and the influence of protein surroundings.[32,33] The excited state dynamics of isolated *B*-LHCII protein was probed over a broad spectral range, 400-950 nm, under selective photoexcitation of Chl *a*, Chl *b*, and Car, so as to catch as many as possible the transient species and to clarify the individual excitation relaxation/transfer pathways. To facilitate the identification of transient species, characteristic absorption spectra of Chl *a* and Chl *b* radical ions in 400-950 nm were measured by means of spectroelectrochemistry (SEC). Owing to the limited structural information of *B*-LHCII, we comparatively measured *S*-LHCII, for which a body of knowledge has been accumulated regarding its structure-function relationship (*vide supra*). For both kinds of LHCIIs, the comprehensive spectral analyses allow us to verify the photoinduced formation of Chl-Chl CT species upon the photoexcitation of Chl Q_y but not Car. To understand such excitation-wavelength

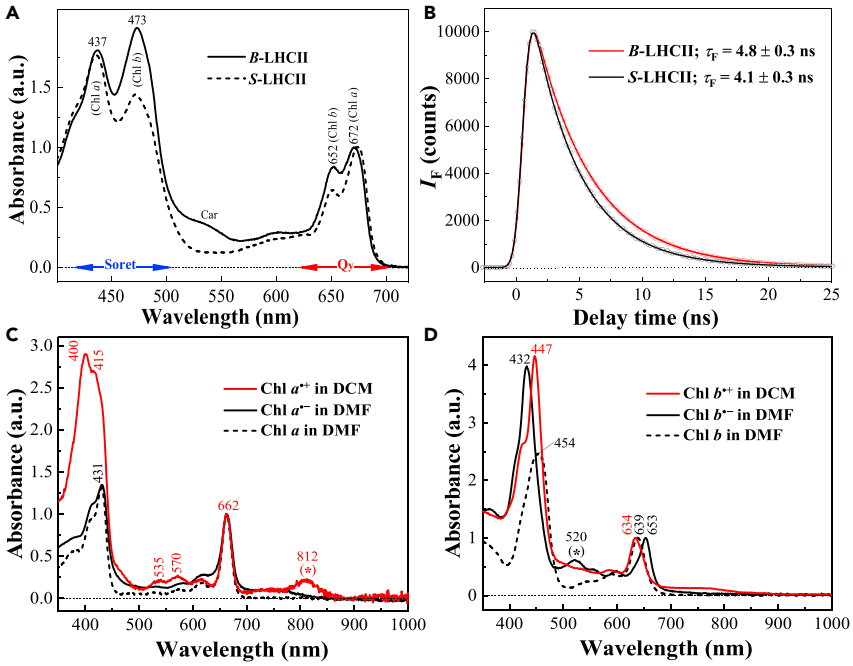

Figure 1. Spectroscopic characterization of *B*-LHCII and Chl radical ions

(A) UV-visible absorption spectra of LHCIIs isolated from *B. corticulans* (*B*-LHCII) and spinach (*S*-LHCII).

(B) Normalized fluorescence kinetics probed at 680 nm. The excitation wavelength was 473 nm. The amplitude-weighted average lifetimes (τ_F)[42] were derived by fitting the decay traces to a bi-exponential model function. (C and D) Optical absorption spectra of Chl *a* (C) and Chl *b* (D) radical ions in organic solvents. Asterisks emphasize the characteristic features. Spectra in panels A, C, and D are normalized at the Q_y band.

dependence, we further measured the absolute fluorescence quantum yield (Φ_{FL}) over a wide spectral range of photoexcitation and discovered the systematic drop of Φ_{FL} and ^{3}Car* production in the Chl Q_y region. Moreover, the Car-to-Chl and the Chl *b*-to-Chl *a* EET processes were confirmed for *B*-LHCII. For the sake of conciseness, we will present the results of *B*-LHCII in this article, while putting those of *S*-LHCII in Supplemental Information for reference when it is needed.

RESULTS

Spectroscopic characterizations of light-harvesting complex II of *Bryopsis corticulans* and chlorophyll radical ions

As seen in Figure 1A, the absorption spectrum of *B*-LHCII exhibits well-separated Chl *a* and Chl *b* absorption in both Soret and Q_y spectral regimes, facilitating selective optical excitation. Compared to *S*-LHCII, *B*-LHCII shows a higher Chl *b*/*a* ratio and enhanced optical absorption in 500-550 nm originating from the keto-Cars, Spx and Spn.[23,25] The Car band peaking around 535 nm resembles that in the absorption spectra of the peridinin-Chl *a* protein (PCP) of dinoflagellates and the fucoxanthin-Chl *a*/*c* protein (FCP) of brown algae, which bind the keto-Cars of peridinin (Per) and fucoxanthin (Fux), respectively. For PCP and FCP, it had been shown that, owing to the strong interactions with the protein surroundings, the $S_2(1B_u^+)$ states of Per and Fux are stabilized substantially, giving rise to the $S_0(1A_g^-)$-to-$S_2(1B_u^+)$ absorption at 535 nm.[34,35] *B*-LHCII contains Spx and Spn as the keto-Cars, thus its 535 nm band most likely has the same origin. Here, it is noteworthy that the Spx-containing LHCII complex from *Codium fragile* also exhibits a distinct absorption around 535 nm, which had been ascribed to the absorptive transition from the $S_0(1A_g^-)$ state to a $^1(n\pi^*)$-type state (S_x) lying between the $^1(\pi\pi^*)$-type $S_1(2A_g^-)$ and $S_2(1B_u^+)$ state based on the fluorescence anisotropy difference between S_x and S_2 (0.3 vs 0.4).[36–38] In addition, time-resolved spectroscopic studies revealed an intramolecular charge transfer (ICT) state (S_{ICT}) for Spn and Spx in solvents,[28,33] which are similar to the cases of other keto-Cars.[39–41] Figure 1B shows the fluorescence decay kinetics of isolated *B*-LHCII and *S*-LHCII proteins recorded under optical excitation at 473 nm, which are similar to those obtained at 440 nm.[25] Compared to *S*-LHCII, the fluorescence lifetime (τ_F)[42] of *B*-LHCII is significantly longer, indicating a less extent of ^{1}Chl* quenching.

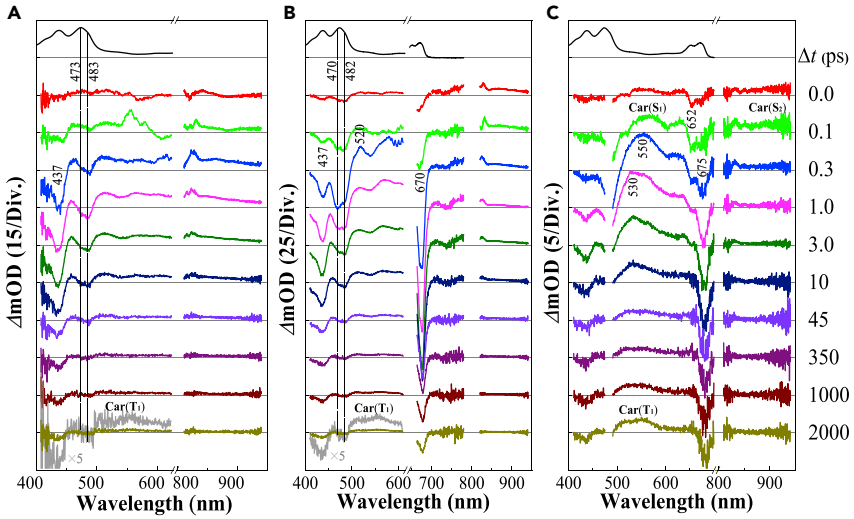

Figure 2. Excited state dynamics of *B*-LHCII

(A-C) The *fs*-TA spectra at selected delay time (Δt) were recorded for *B*-LHCII under photoexcitation of (A) Chl *a* at 675 nm, (B) Chl *b* at 640 nm, and (C) Car at 485 nm. Blank sections are due to the interference from the actinic laser and the laser at 800 nm for the generation of the white-light probe. For reference, a steady-state absorption spectrum is shown on the top of each panel.

To assist the subsequent TA-spectral analysis, we measured the SEC spectra of Chl *a* and Chl *b* radical ions, and the results are shown in Figures 1C and 1D, respectively. The spectra of Chl $a^{\bullet+}$, Chl $a^{\bullet-}$, and Chl $b^{\bullet+}$ are in well agreement with those documented,[43,44] whereas the Chl $b^{\bullet-}$ spectrum has not been reported before (cf. Figure 1D). These spectra can be characterized in terms of different spectral regions. (i) 400-700 nm. Despite the differences in amplitudes and in maximal wavelengths, the radical ions of Chl *a* and Chl *b* retain the general absorption features of their neutral forms, i.e. their SEC spectra are characterized by the Soret bands (350-450 nm) and the Q_y bands (630-660 nm) along with vibronic features (500-650 nm). In Figure 1D, Chl $b^{\bullet-}$ exhibits a distinctive absorption feature at 520 nm, which is absent in the other SEC spectra. In addition, its Q_y band is red-shifted for 14 nm and 19 nm with reference to those of neutral Chl *b* and Chl $b^{\bullet+}$ respectively, whereas no such redshifts are seen in the spectra of Chl *a*. (ii) 700-1000 nm. Chl $a^{\bullet+}$ and Chl $b^{\bullet+}$ absorb with significant amplitudes, whereas their anionic counterparts absorb relatively weaker. Notably, Chl $a^{\bullet+}$ exhibits a characteristic band at 812 nm, whereas Chl $b^{\bullet+}$ shows a red tail decaying almost monotonically. The near-infrared absorption maximum of Chl $a^{\bullet+}$ is known to be solvent-dependent but nearly independent of its counterion.[43–45]

Excited-state dynamics of light-harvesting complex II of *Bryopsis corticulans*

Figures 2A–2C displays the representative *fs*-TA spectra of *B*-LHCII recorded under selective photoexcitation of Chl *a*, Chl *b*, and Car, respectively. More details of the spectral evolution in the initial 1 ps are presented in Figures S1A-S1C. Hereafter, we shall first characterize the spectra under Chl *a* Q_y-excitation, wherein the simplest excited-state dynamics are expected because of the low excitation photon energy (cf. Scheme 1)

Excited-state dynamics under chlorophyll *a* Q_y-excitation (Figure 2A)

The *fs*-TA spectra exhibiting negative ground-state bleaching (GSB) and positive excited-state absorption (ESA) can be characterized by 3 successive temporal phases.

(i) 0.0-1.0 ps. Despite the low excitation photon energy, Chl *b* GSB at 473/483 nm appeared concomitantly with Chl *a* GSB at 437 nm (see Figure S1A for more details). At the excitation wavelength of 675 nm, the appearance of Chl *b* GSB can be due to the inhomogeneity of the Chl *b* Q_y band, which resulted in the photoexcitation of red-absorbing Chl *b* in view of the 10 nm bandwidth of the pump laser. This is in line with the distinct split of the Chl *b* Q_y band (650/658 nm) in the absorption spectrum of *B*-LHCII at 77 K.[24] However, it is seen in Figure 2A that Chl *b* and Chl *a* GSBs evolve in phase, lacking any kinetic correlation that may stem from the Chl *b*-to-Chl *a* EET process. The sizable Chl *b* GSB and the in-phase GSB recovery of

Chl *a* and Chl *b* are unique to *B*-LHCII bearing a relatively high Chl *b*/*a* ratio, as *S*-LHCII excited at 675 nm exhibited an almost unrecognizable Chl *b* GSB at 471 nm along with a weak Chl *b* GSB at 485 nm, both of which appeared as weak dips superimposed with a broad ESA background (cf. Figure S1D). In 500-600 nm, the broad ESA mainly originates from Chl *a*-related transient species. In 800-950 nm, the ESA around 820 nm resembles the characteristic Chl $a^{\bullet+}$ absorption spectrum (Figure 1C). In this context, the Chl $a^{\bullet+}$ absorption at 820 nm had been reported for PSII core complexes.[45] Therefore, the near-infrared signature in Figure 2A indicates the photogeneration of CT species involving Chl $a^{\bullet+}$. It is noteworthy that *S*-LHCII also exhibited such a near-infrared feature (Figures S1D and S2A), however, the ESA (500-600 nm) differs completely from that of *B*-LHCII, likely due to the electronic interaction between ^{1}Chl *a** and lutein having a comparable S_1-state energy.[24,32]

(ii) 1.0-45 ps. The near-infrared ESA in 800-950 nm decayed in phase with Chl *a* and Chl *b* GSBs in 400-500 nm, which is due to the charge recombination between Chl $a^{\bullet+}$ and Chl $a^{\bullet-}$. The synchronous GSB evolution of Chl *a* and Chl *b* suggests the involvement of Chl $b^{\bullet-}$ as a counterion in charge recombination with Chl $a^{\bullet+}$. The ESA (800-950 nm) lasting until sub-nanosecond originates neither from the Car($S_n \leftarrow S_2$) absorption known to be ultrashort lived (<200 fs),[46,47] nor from the Car$^{\bullet+}$($D_n \leftarrow D_0$) absorption having completely different spectral patterns.[45,48,49]

(iii) 45-2000 ps. The *fs*-TA spectra evolve without appreciable spectral variation, except the emerging of Car($T_n \leftarrow T_1$) ESA in 500-600 nm as shown by the blowup spectrum at 2000 ps (Figure 2A). The dual ESA bands of Car(T_1) are characteristic to ^{3}Spn* (505 nm) and ^{3}Spx* (550 nm), respectively.[25] In plant LHCIIs, the photosensitized formation of ^{3}Car* proceeds in a sub-nanosecond timescale owing to the wavefunction overlap between ^{3}Chl* and Car,[50,51] which is much faster than the timescale of bacterial light-harvesting complexes (10-20 ns).[52] Based on the ESA at 820 nm, the in-phase evolution of Chl GSBs and the identification of Chl radical ions (i—iii), we propose the ultrafast photogeneration of Chl-Chl CT species.

Excited-state dynamics under chlorophyll *b* Q_y-excitation (Figure 2B)

Immediately following the pulsed photoexcitation at 640 nm (Δt = 0.0-0.1 ps), Chl *b* GSB showed up at 470/482 nm, while weaker Chl *a* GSBs at 437 nm and 672 nm appeared owing to a minor excitation of Chl *a* and/or the fastest phase of Chl *b*-to-Chl *a* EET with a time constant of ~100 fs.[16,53] Subsequently, a slower phase of Chl *b*-to-Chl *a* EET can be recognized from the correlation between the decay of Chl *b* GSB at 470 nm and the rise of Chl *a* GSB at 437 nm as seen more clearly in Figure S1B. However, a similar phase of Chl *b*-to-Chl *a* EET was not observed in the case of Chl *a* Q_y-excitation. Most importantly, the prominent ESA peak at 520 nm (Δt = 0.1-1.0 ps, see Figure S1B for more details), not seen in the case of Chl *a* Q_y-excitation, agrees well with the characteristic Chl $b^{\bullet-}$ absorption at 520 nm (Figure 1C). Such a spectral similarity together with the 820 nm signature of Chl $a^{\bullet+}$ prove the involvement of Chl $a^{\bullet+}$-Chl $b^{\bullet-}$ CT species. As shown in Figures S1E and S2B, *S*-LHCII also exhibited ESAs at 520 nm and 800-950 nm, implying the involvement of Chl $a^{\bullet+}$-Chl $b^{\bullet-}$ CT species. However, the ESA of *S*-LHCII at 520 nm is considerably weaker and is superimposed with the broad ESA background that is drastically different from the case of *B*-LHCII (Figures S1E and S1B). For both kinds of LHCIIs, the 520 nm feature of Chl $b^{\bullet-}$ decayed out in 1 ps, which can be ascribed to the ultrafast charge recombination reaction. In the later phase (Δt = 1.0-2000 ps), the spectral dynamics are essentially the same as that under Chl *a* Q_y-excitation.

Excited-state dynamics under carotenoid-excitation (Figure 2C)

Optical excitation of *B*-LHCII at 485 nm promoted Spn and Spx from the $S_0(1A_g^-)$ to the $S_2(1B_u^+)$ state, as well as a minor portion of Chl *b* from the S_0 to the B_x/B_y states. The *fs*-TA spectra are distinctly different from those upon Chl Q_y-excitation (Figure 2C vs Figures 2A and 2B).

(i) 0.0-1.0 ps. In 500-650 nm, prominent ESA bands with maxima at 530 nm and 550 nm and spectral extension to 650 nm are observed. The maxima and the broad extension are characteristic of the concomitant occurrence of ESA($S_n \leftarrow S_1$) and ESA($S_n \leftarrow S_{ICT}$) for keto-Cars such as Spx and Spn. Based on a detailed fs-TA study on the solvent effect on the excited-state dynamics of Spx and Spn,[33] and in view of the evolution-associated difference spectra (EADSs) derived from global analysis (*vide infra*), we attribute the ESAs peaking at 530 nm and 550 nm to Spx and Spn, respectively. In 650-700 nm, the recovery of Chl *b* GSB at 652 nm correlates with the rise of Chl *a* GSB at 675 nm (see Figure S1C for more details), reflecting the Chl *b*-to-Chl *a* EET process. In 850-950 nm, the broad ESA decaying in 1 ps is dominated by Car($S_m \leftarrow S_2$) absorption.[46,47] This assignment draws support from the 850-900 nm kinetic trace in Figure 4C, which is distinctly

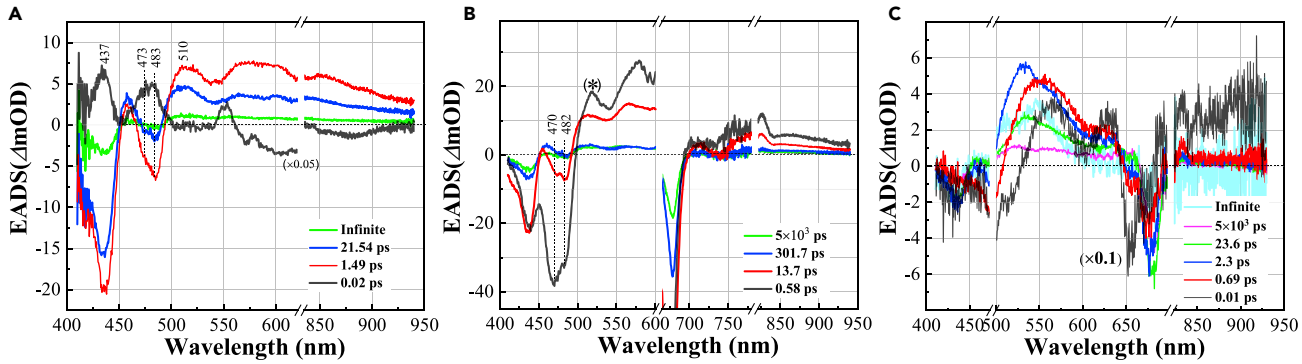

Figure 3. Evolution associated difference spectra (EADSs)

(A-C) Evolution-associated difference spectra (EADSs) of transient species involved in *B*-LHCII under photoexcitation of (A) Chl *a* at 675 nm, (B) Chl *b* at 640 nm, and (C) Car at 485 nm.

different from the 825/900 nm traces recorded under Chl Q_y-excitation (Figures 4A and 4B). The correlation of ESA (850-950 nm) decay with ESA (500-650 nm) rise, as may be discerned more clearly from Figure S1C, indicates the process of Car($S_2 \rightarrow S_1$) internal conversion.

(ii) 1.0−2000 ps. The decay of Car($S_n \leftarrow S_1$) ESA in 500-650 nm correlates with the rise of Chl *a* GSB (437/675 nm), reflecting the EET process from the S_1 state of Spn and/or Spx to the Q_y state of Chl *a*. In the case of the Car-excitation of *S*-LHCII, the process of Car(S_1)-to-Chl *a*(Q_y) EET was not obvious (Figures S2C and S4C). In Figure 2C, the Car($S_m \leftarrow S_2$) ESA in 850-900 nm decayed out in 1 ps, which is much faster than the decay of ESA (850-900 nm) upon Chl Q_y-excitation. Later than 45 ps, the spectral evolution is similar to the cases of Chl Q_y-excitation, except for the much more intense ESA of Car(T_1) in 350-2000 ps. For reference, *S*-LHCII photoexcited at 485 nm showed similar spectral dynamics except for substantially narrower Car($S_n \leftarrow S_1$) and Car($T_n \leftarrow T_1$) ESAs originating from lutein (Figure S2C). Most importantly, the near-infrared spectral feature of Chl-Chl CT species was negligible for both *B*-LHCII and *S*-LHCII under Car-excitation.

Kinetic schemes of light-harvesting complex II of *Bryopsis corticulans*

To see the key spectral features of different transient species, we derived the EADSs from the *fs*-TA datasets as shown in Figure 2 on the basis of an irreversible sequential kinetic model,[54] and the results are shown in Figure 3. In the case of Chl *a* Q_y-excitation (Figure 3A), the EADS in black can be ascribed to a rise component of excited-state Chls judging from the inverted spectral features of Chl GSB (437/473/483 nm) and ESA (600 nm). The EADSs in red and in blue can be assigned to the Chl-Chl CT species, Chl $a^{\bullet+}$-Chl $a^{\bullet-}$, as supported by the characteristic near-infrared features of Chl radical ions. This pair of EADSs, decaying with the respective time constants of 1.49 and 21.54 ps, reflect the dual phases of charge recombination. The EADS in green living pseudo-infinitely long can be ascribed to ^{1}Chl *a**, whose fluorescence lifetime was determined to be 4.8 ns (Figure 1C).

In the case of Chl *b* Q_y-excitation (Figure 3B), the EADS in black (0.58 ps) with characteristic Chl $b^{\bullet-}$ absorption at 520 nm is assigned to Chl $a^{\bullet+}$-Chl $b^{\bullet-}$, while the EADS in red (13.7 ps) can also be attributed to Chl $a^{\bullet+}$-Chl $b^{\bullet-}$ in view of the concomitant evolution of Chl *a* and Chl *b* GSBs. The successive EADS in blue (300 ps) can be attributed to Chl *a*-Chl *a* CT species, and the EADS in green (5 ns) having a similar shape as that in Figure 3A can be ascribed to ^{1}Chl *a**.

Under Car-excitation (Figure 3C), the EADSs are completely different from those upon Chl Q_y-excitation in both visible and near-infrared regions. The EADS in black agrees with the Car($S_m \leftarrow S_2$) ESA characterized by broad near-infrared absorption extending over 900 nm.[47] The rather short decay time constant of 10 fs, within the limit of time resolution (120 fs), is indicative of the involvement of the Car(S_2)-to-Chl EET process (*vide infra*). In the range of 800-950 nm, the other 4 EADSs show extremely low amplitudes, implying that the production of Chl-Chl CT species is negligibly low. The EADSs in Figure 3C, including those in red (0.69 ps), blue (2.3 ps), and green (23.6 ps), all exhibit the ESA features of ^{1}Spx* and ^{1}Spn* characterized by the respective maxima at 530 nm and 550 nm, as revealed by a recent *fs*-TA study of Spn and Spx in organic

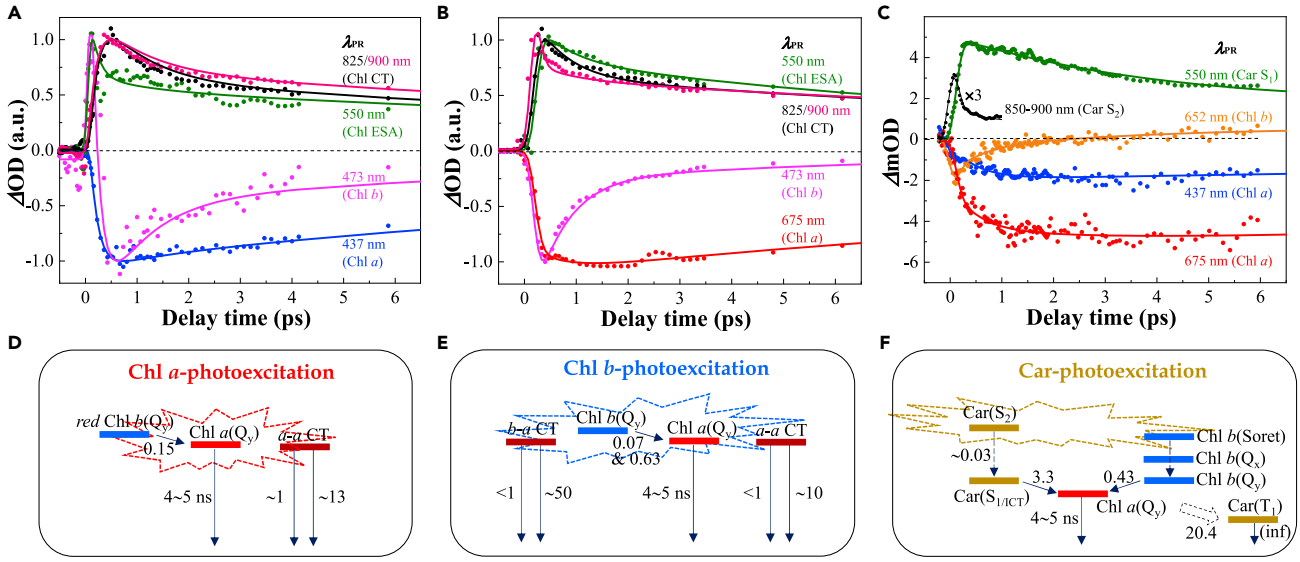

Figure 4. Kinetic schemes of *B*-LHCII

(A-C) Kinetic traces at selected probing wavelengths (λ_{PR}) for *B*-LHCII under the photoexcitation of (A) Chl *a* at 675 nm, (B) Chl *b* at 640 nm, and (C) Car at 485 nm. They were plotted from the respective *fs*-TA datasets of Figure 2. In panels A and B, the kinetic traces are normalized. Solid lines are fitting curves (see text for details).

(D-F) The corresponding kinetic schemes proposed based on the results of curve fitting and EADS analysis. Numerals represent the time constants in ps.

solvents.[33] In addition, the spectra in 550-650 nm can be assigned to the ESA ($S_N \leftarrow S_{ICT}$) of the keto-Cars. As proposed in ref.[33], the S_{ICT} state can promote the Car-to-Chl EET. The decay time constants of ^{1}Spn* (red EADS, 0.69 ps) and ^{1}Spx* (blue EADS, 2.3 ps) are both substantially shorter than the $S_{1/ICT}$ lifetime in absence of energy acceptor, i.e. 10-20 and 60 ps in polar and nonpolar solvents, respectively.[28,33] Such lifetime shortening suggests that both Spn and Spx are involved in Car($S_{1/ICT}$)-to-Chl EET. In the case of *S*-LHCII, only the S_1 state of Lut620 plays a significant role in Car-to-Chl EET,[9] and this is also supported by our global analysis results (Figure S3C). In Figure 3C, the EADSs in black and in red show distinct Chl *b* GSB at 650 nm, whereas those in blue and in green exhibit prominent Chl *a* GSB at 675 nm. Moreover, the recovery of Chl *b* GSB corresponds to the rise of Chl *a* GSB in a multiphasic manner, suggesting the inhomogeneity of the Chl *b*-to-Chl *a* EET process. The time constants, 10 fs, 0.69 ps, and 2.3 ps, are in agreement with those reported in ref.[16] and ref.[53]. As for the later EADSs, the pink one represents ^{1}Chl *a** relaxing with a time constant of 5 ns, while the cyan one stands for the ESA ($T_n \leftarrow T_1$) of Spn and Spx peaking at 505 nm and 550 nm, respectively.[25]

In view of the complexity of LHCII dynamics that obviously surpasses a sequential kinetic scheme, the EADSs in Figure 3 can be used merely as a guide for more implicit kinetic analysis. We then plotted the kinetic traces at representative probing wavelengths directly from the *fs*-TA datasets and fitted them simultaneously to a model function consisting of 4 or 5 exponential components (cf. Figures 4A–4C). The decay time constants and the preexponential amplitudes derived for *B*-LHCII upon Chl *a*, Chl *b*, and Car photoexcitation, respectively, are summarized in Tables S1–S3. On the basis of the timescales and the amplitude polarities in tables, and with reference to the above EADS results, we further propose the following kinetic schemes for *B*-LHCII under selective photoexcitation (Figures 4D–4F).

Photogenerated chlorophyll-chlorophyll charge transfer species and Chl *b*-to-Chl *a* excitation energy transfer

Figures 4A and 4B show the kinetic traces of *B*-LHCII photoexcited at Chl Q_y-bands, which probe Chl *a* GSB at 437/675 nm, Chl *b* GSB at 473 nm, Chl ESA at 550 nm, and Chl radical ions at 825/900 nm. As Chl *a* Q_y-excitation would not arouse any excitation of Car owing to low photon energy, the kinetic traces in Figure 4A can be well described by a four-exponential model function. The leading edges of the kinetics at 437/825/900 nm rise within the limit of time resolution, implying the instantaneous Chl *a* bleaching and Chl $a^{\bullet+}$-Chl $a^{\bullet-}$ formation upon photoexcitation at 675 nm. The oscillation feature of the 473 nm trace

observed before 0.5 ps is due to the rapid change of ESA polarity as seen from the original *fs*-TA spectra (Figure S1A, Figure 2A). Figure 4D shows the kinetic scheme proposed for this case: Pulsed optical excitation at 675 nm promptly generates the Chl $a^{\bullet+}$-Chl $a^{\bullet-}$ species, which recombines in a biphasic manner with the respective time constants of ~1 and ~13 ps. Based on the curve fitting parameters (cf. Table S1), an EET process from red-absorbing Chl *b*(Q_y) to Chl *a*(Q_y) can be assumed, whose time constant of 0.15 ps agrees with that of Chl *b*-to-Chl *a* EET as reported for *S*-LHCII.[16,53]

In the case of Chl *b* Q_y-excitation (Figure 4B), the decay of the 473 nm trace apparently correlates with the rise of the 675 nm trace, proving the Chl *b*-to-Chl *a* EET reaction. The kinetic traces in Figure 4B can be best described by a five-component exponential model function. The component with a time constant of 0.07 ps, not identified by EADS analysis, can be ascribed to Chl *b*-to-Chl *a* EET. On the other hand, in Figure 3B the fastest-evolving EADS (black) exhibits the characteristic Chl $b^{\bullet-}$ absorption at 520 nm along with the intense GSBs of Chl *a* and Chl *b* in 400-500 nm, which together with the 800-950 nm ESA prove the photogeneration of Chl $a^{\bullet+}$-Chl $b^{\bullet-}$. The curve-fitting combined with the EADS results allows us to propose the kinetic scheme as delineated in Figure 4E, which is characterized by the involvement of both Chl $a^{\bullet+}$-Chl $b^{\bullet-}$ and Chl $a^{\bullet+}$-Chl $a^{\bullet-}$ species.

Carotenoid-to-chlorophyll excitation energy transfer

Figure 4C shows the kinetic traces recorded for *B*-LHCII under Car-excitation, which are obviously different from those under Chl Q_y-excitation (Figures 4A and 4B). For instance, the kinetic trace of 850-900 nm day extremely fast, and the Chl *a* GSB at 437/675 nm rises in a multiphasic manner. As mentioned above, the 850-900 nm trace probes the Car($S_m \leftarrow S_2$) absorption, which is in accord with the fastest-evolving EADS (black, Figure 3C). Figure 4F depicts the proposed kinetic scheme: The Car($S_2 \rightarrow S_1$) internal conversion proceeds in ~30 fs, a timescale agrees with the S_2-state lifetime of ~35 fs as determined by ultrafast time-resolved fluorescence spectroscopy for the Spx-containing LHCII of *Codium fragile*.[36] In ref.[36], it was concluded that the S_2 state is not involved in Car-to-Chl EET and that the Car(S_x)-to-Chl(Q_x) EET proceeds with a time constant of ~110 fs. Regarding the Car(S_1)-to-Chl(Q_y) EET pathway in *B*-LHCII, a rise phase with a time constant of 3.3 ps was identified in the Chl *a* GSB at 437/675 nm, which correlates with the decay phase in the Car(S_1) kinetics at 550 nm. The EET time constant, 3.3 ps, is consistent with the Car-to-Chl EET time constants derived from EADS analysis (Figure 3C), i.e. 0.69 and 2.3 ps for Spn and Spx, respectively. The Car-Chl EET observed for *B*-LHCII can be rationalized as the followings. Spn and Spx in the central domain of *B*-LHCII occupy the Lut620 and the Lut621 sites, respectively. Since the interaction network in the Car binding pockets is relatively insensitive to the chemical structure of the embedded Car,[55] Spn and Spx in *B*-LHCII are expected to keep similar distances from the nearby Chls as Luts do in *S*-LHCII. In the case of *S*-LHCII, the closest edge-to-edge distances of Lut620-Chl *a*610 and Lut621-Chl *a*602 are 3.53 Å and 3.37 Å, respectively, which may allow ultrafast Car-Chl EET.[9,56]

Carotenoid triplet production and absolute fluorescence quantum yield

The photosensitized formation of ^{3}Car* in *B*-LHCII is validated by the transient spectra at 1-2 ns (Figure 2, blowup spectra of Car(T_1)). Figure 5A shows the 505 nm kinetic traces in this temporal regime, illustrating the formation of ^{3}Spn* at different excitation wavelengths (λ_{EX}). Obviously, the Car excitation at 485 nm led to a substantially higher ^{3}Spn* production than the Chl Q_y-excitation did, which is corroborated by the EADS in cyan in Figure 3C. The 550 nm kinetic traces of ^{3}Spx* at different λ_{EX} are similar to the 505 nm ones (data not shown). On the other hand, the ^{3}Lut* kinetic trace at 507 nm for *S*-LHCII exhibits similar excitation-wavelength dependence, i.e. Car-excitation compared to Chl Q_y-excitation resulted in faster ^{3}Lut* formation with a considerably higher population (Figure S5).

Regarding the extent of fluorescence quenching, the Φ_{FL} of *B*-LHCII (30%) is significantly higher than that of *S*-LHCII (25%) as seen from Figure 5B, in accord with the longer fluorescence lifetime of *B*-LHCII than that of *S*-LHCII (cf. Figure 1B). For both *B*-LHCII and *S*-LHCII, the Φ_{FL} remains constant in 430-600 nm, but it declines progressively from 600 nm to 650 nm. Moreover, to the long-wavelength limit, the Φ_{FL} of *B*-LHCII and *S*-LHCII tend to converge with each other. Most importantly, both Φ_{FL} and ^{3}Car* yield correlate with the photogeneration of Chl-Chl CT species, i.e. the Chl Q_y-excitation boosts the production of Chl-Chl CT species, whereas it suppresses both Φ_{FL} and ^{3}Car* yield. On the contrary, the Car-excitation suppresses the formation of Chl-Chl CT species, whereas it enhances the yields of Chl-fluorescence and ^{3}Car*. Under red-light illumination in Chl Q_y spectral regime, the inverse correlation between charged and neutral

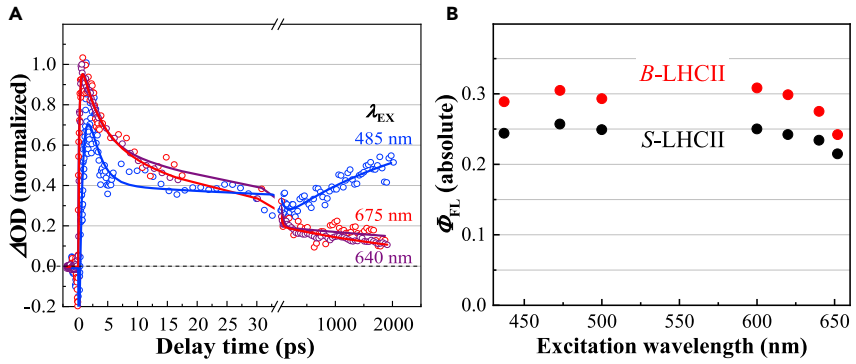

Figure 5. ^{3}Car* production and absolute fluorescence quantum yield

(A) Kinetic traces probed at 505 nm for *B*-LHCII photoexcited at indicated excitation wavelengths (λ_{EX}). They were obtained from the respective *fs*-TA spectra as shown in Figure 2.

(B) Absolute fluorescence quantum yields (Φ_{FL}) of *B*-LHCII and *S*-LHCII plotted against excitation wavelength. Each value was an average of three independent measurements.

transient species of Chl points to the role of Chl-Chl CT state in quenching ^{1}Chl*, which seems to be common for the algal and the plant LHCIIs.

DISCUSSION

In the present work, the broad *fs*-TA spectral window allows the detection of different kinds of transient species, and hence the dynamics of excitation conversion, transfer, and relaxation among different pigments can be comprehensively examined. It is understandable that *B*-LHCII on Chl Q_y-excitation exhibits relatively simple excitation dynamics because the Car having higher optical transition energy cannot be directly excited (cf. Scheme 1). The simplicity of *B*-LHCII excitation dynamics is manifested by comparing to the case of *S*-LHCII under Chl Q_y-excitation, wherein the *fs*-TA spectra show somewhat Chl-Lut entangled dynamics in the visible spectral region (Figures 2 vs S2). We will hereafter focus on discussing the excited-state dynamics of *B*-LHCII.

Excitation-wavelength dependent formation of chlorophyll-chlorophyll charge transfer species

Historically, several forms of CT species were reported for plant LHCs. For instance, it was found that Chl Q_y-excitation of thylakoid membranes or monomeric LHCII (CP29, CP26, and CP24) yields $Car^{\bullet+}$ in a sub-picosecond timescale. This together with the subsequent $Car^{\bullet+}$-$Chl^{\bullet-}$ charge recombination in 150-200 ps was proposed to be an effective qE mechanism.[57–59] However, $Chl^{\bullet-}$ as a counterion has not been observed, despite the successful detection of the near-infrared spectral signature of $Car^{\bullet+}$. For trimeric LHCII in the qE state, it has been theoretically shown that the Lut620-Chl *a*612 CT interaction can fully account for the quenching of ^{1}Chl*, because this CT state is isoenergetic with the Q_y state of *a*612 belonging to the terminal emitting Chl *a* cluster {*a*610, *a*611, *a*612}.[17,60] It is noteworthy that the photoinduced formation of $Car^{\bullet+}$ has not been observed for LHCII in the energy-quenched state. This is also true in the present work for the LHCII in the light-harvesting state: For both *B*-LHCII and *S*-LHCII, the characteristic near-infrared ESAs of Chl ionic radicals and/or Car $S_2(1B_u^+)$ state were observed, however, no spectral indication of $Car^{\bullet+}$ was discerned in the near-infrared region (Figures 2, S1 and S2). On the other hand, the Chl-Chl CT states of the terminal emitting Chl *a* cluster, such as *a*610$^{\bullet+}$-*a*612$^{\bullet-}$ and *a*610$^{\bullet+}$-*a*611$^{\bullet-}$, had been proposed to be the qE mediators on the basis of the kinetic heterogeneity of the excited states of aggregated and crystalline LHCIIs at cryogenic temperatures (see ref. [61] and ref. [62]).

In addition to the neutral excited-state species of Chl and Car, the present work has identified the Chl radical ions in isolated LHCII proteins based on the selective photoexcitation and the broadband *fs*-TA, as well as on the SEC spectroscopic characterization of Chls. The results prove unambiguously the involvement of Chl $a^{\bullet+}$ and Chl $b^{\bullet-}$ for both *B*-LHCII and *S*-LHCII upon Chl Q_y-excitation. In addition, it is shown that the direct photoexcitation of Car generates Car $S_2(1B_u^+)$ state rather than Chl radical ions. The red-light induced formation of Chl-Chl CT species can be explained by invoking the mechanism of state mixing between exciton and CT-state of tightly packed Chls.[63,64] Such a state-mixing state, as also reported for

plant LHCIIs,[65] can be coherently created by Chl Q_y-excitation, but cannot be populated via incoherent Car-to-Chl EET. In this context, the photoinduced Chl *a*-to-Chl *b* electron transfer reaction holds an energetic basis, i.e., for a coupled Chl *a*-Chl *b* pair, the driving force of the forward reaction is about 3-folds of that of the reverse one.[29] In addition, the preference for heterodimer over homodimer in CT formation draws support from recent theoretical work on plant LHCIIs, i.e., the free energy driving the formation of *a*603$^{\bullet+}$-*b*609$^{\bullet-}$ is somewhat larger than that of *a*612$^{\bullet+}$-*a*611$^{\bullet-}$.[17] Experimentally, recent 2D electronic spectroscopy (2DES) on *S*-LHCII trimer at 77 K has provided evidence for coherent mixing of *a*602-*a*603 exciton with *a*603-*b*609 CT state.[65] In the case of *B*-LHCII, a higher Chl *b*/*a* ratio implies more heterodimeric CT sites compared to the case of *S*-LHCII. This is indeed the case as evidenced by the more prominent Chl $b^{\bullet-}$ signature at 520 nm in the *fs*-TA spectra of *B*-LHCII (Figure S1B) compared to *S*-LHCII (Figure S1E).

The fluorescence lifetime of Chl *a* in organic solvents varies from 5 ns to 7 ns.[31,66–68] It decreases to 4.8 and 4.1 ns, respectively, for isolated *S*-LHCII and *B*-LHCII in the light-harvesting state, and further to sub-nanoseconds for these LHCIIs in the qE state.[4,69] The present work discovers, for the target LHCIIs, the ultrafast photoinduced formation of Chl $a^{\bullet+}$-Chl $a^{\bullet-}$ and Chl $a^{\bullet+}$-Chl $b^{\bullet-}$ charge pairs, as well as the subsequent charge recombination proceeding in ps-ns timescales, which can be connected to the quenching of ^{1}Chl*. However, this mechanism is not necessarily to be a qE-component of NPQ, because the LHCIIs in question are in the light-harvesting state and, compared to *S*-LHCII, *B*-LHCII with more Chl $a^{\bullet+}$-Chl $b^{\bullet-}$ species exhibits a higher Φ_{FL} and a longer fluorescence lifetime. Obviously, the LHCIIs in the energy-quenched state must be examined, so as to derive further information concerned with the role of Chl-Chl CT species.

Despite a subtle variation in molecular structures, Chl *b* differs considerably from Chl *a* in excited-state energetics and dynamics such as energy levels, fluorescence, and triplet yields, as well as intrinsic nonradiative relaxation.[29,30] In addition, Chl *b* is known to be both structurally and functionally essential for LHCs.[70] For instance, it enhances light harvesting by broadening the cross-section of light absorption, which is in line with the relatively high Chl *b*/*a* ratio of the LHCII of *B. corticulans*. In addition, the extra Chls *b* may downregulate the electronic coupling strength among Chls by introducing more energetic disorders, and thereby affect the energy levels responsible for the nonradiative deactivation of ^{1}Chl*.[16] This can be connected to a significantly higher Φ_{FL} of *B*-LHCII than that of *S*-LHCII (Figure 5B).

Carotenoid-to-chlorophyll excitation energy transfer and carotenoid triplet formation

For plant LHCIIs, extensive experimental and theoretical studies have been carried out to understand the EET mechanism among specific lutein and Chl cofactors.[9,11,16,56,71,72] For LHCIIs in light-harvesting conformation, recent ultrafast time-resolved Raman spectroscopy has shown that the Lut621(S_1)-to-Chl(Q_y) and Lut620-to-Lut621 EET pathways are inactive,[9] in contrast to the role of Lut621 in promoting Car-to-Chl EET as proposed on the basis of ultrafast 2DES studies.[56] For *B*-LHCII equipped with Spn and Spx at the respective Lut620 and Lut621 sites,[23,25] the present work proves that both Spn and Spx are involved in the Car($S_{1/ICT}$)-to-Chl *a*(Q_y) EET with a time constants of 3.3 ps (cf. Figure 4F), and that Chl *b* transfers singlet excitation to Chl *a*(Q_y) in sub-picosecond timescales in a multiphasic manner. Therefore, the pair of keto-Cars and Chl *b* as accessary and major light-harvesters, respectively, can help *B. corticulans* to harness the water penetrating sunlight in the blue-green spectral regime.

The kinetics of ^{3}Car* formation in plant LHCIIs had been found to parallel the kinetics of ^{1}Chl *a** relaxation, indicating an extremely high efficiency of Chl *a*-to-Car triplet EET.[50,51] The same is true for *B*-LHCII as seen from the *fs*-TA data in Figure 2. ^{3}Spn* at 505 nm and ^{3}Spx* at 550 nm with comparable amplitudes can be recognized later than 350 ps, implying that both Spn and Spx are capable of efficiently quenching ^{3}Chl*. It is rather intriguing to see the inverse correlation between the charged and the neutral species of Chls for *B*-LHCII and *S*-LHCII under red-light excitation, i.e., when the excitation wavelength was extended into the Chl Q_y region, the production of Chl-Chl CT species increased whereas Φ_{FL} and ^{3}Car* production decreased (Figures 5 and S4). This points to the role of Chl-Chl CT interaction in deactivating ^{1}Chl*, which readily explains the concomitant decrease in Φ_{FL} and ^{3}Car* yield. On the other hand, Car-excitation in the blue-green spectral region yields negligible Chl-Chl CT species and relatively high Φ_{FL} and ^{3}Car* yield, which is also corroborative to the deactivation of ^{1}Chl* via Chl-Chl CT reaction. Here, it is worthy of noting the followings: (i) Under Chl Q_y-excitation and with reference to *B*-LHCII, *S*-LHCII having a lower Chl *b*/*a* ratio (and less Chl $a^{\bullet+}$-Chl $b^{\bullet-}$ formation) exhibits a lower Φ_{FL} (and a shorter fluorescence lifetime), meaning a higher extent of quenching ^{1}Chl*. (ii) The excited-state dynamics of *S*-LHCII originate from Chl species with involving of Chl-Lut interaction. This is validated by comparing the transient spectra of *S*-LHCII

(Figures S2A and S2B) with those of *B*-LHCII dominated by Chl species (Figures 2A and 2B). (iii) Similar to *S*-LHCII, *B*-LHCII on aggregation exhibits a sub-nanosecond fluorescence lifetime, meaning a substantial extent of energy quenching. Taken together, it is hardly to relate the photogeneration of the Chl-Chl CT state to the qE behavior at the present stage, and hence it is absolutely needed to further examine the excited-state dynamics of *B*-LHCII in the energy-quenched state. Nevertheless, as for *B*-LHCII under Chl Q_y-excitation, Spn, and Spx do not contribute to the excited-state dynamics, we suggest that the Chl-Chl CT interaction can fully account for the nonradiative deactivation of ^{1}Chl* in *B*-LHCII.

In conclusion, we have investigated, with comparison to spinach LHCII, the ultrafast excited-state dynamics of *B. corticulans* LHCII under the selective photoexcitation of Chl *a*, Chl *b*, and Car, respectively. The transient species were probed in visible-to-near infrared spectral regions with *fs*-TA, which together with the characteristic optical absorption spectra of Chl radical ions obtained by SEC allow us to identify Chl $a^{\bullet+}$-Chl $a^{\bullet-}$ and Chl $a^{\bullet+}$-Chl $b^{\bullet-}$ charge pairs in both kinds of LHCIIs upon Chl Q_y-excitation but not Car-excitation. These Chl-Chl CT species form in an ultrafast timescale (<120 fs) and recombine in a biphasic manner with the respective time constants of sub-picosecond and a few tens of picoseconds (10-50 ps). The photogeneration of Chl-Chl CT species was found to inversely correlate with the absolute fluorescence quantum yield (Φ_{FL}) and the ^{3}Car* production. We propose that the red-light induction of Chl-Chl CT species is a general occurrence of both algal and plant LHCIIs in light-harvesting form. The present work also confirmed the Car-to-Chl and Chl *b*-to-Chl *a* EET reactions in *B*-LHCII proceeding with the time constants of 3.3 ps and <1 ps, respectively, which facilitates the marine green alga *B. corticulans* to harvest water penetrative blue-green sunlight.

Limitations of the study

Further investigation on algal and plant LHCIIs in energy-quenched state and/or on their Chl *b*-deficient mutants is needed to clarify the possible involvement of Chl-Chl CT state in the qE mechanism of NPQ.

STAR★METHODS

Detailed methods are provided in the online version of this paper and include the following:

- KEY RESOURCES TABLE
- RESOURCE AVAILABILITY
  - Lead contact
  - Materials availability
  - Data and code availability
- EXPERIMENTAL MODEL AND SUBJECT DETAILS
- METHOD DETAILS
  - Sample preparation
  - Absorption spectra
  - Fluorescence spectroscopies
  - Spectroelectrochemical (SEC) spectroscopy
  - Femtosecond time-resolved absorption (*fs*-TA) spectroscopy
- QUANTIFICATION AND STATISTICAL ANALYSIS

SUPPLEMENTAL INFORMATION

Supplemental information can be found online at https://doi.org/10.1016/j.isci.2022.105761.

ACKNOWLEDGMENTS

We would like to thank Ying-Chao Ma for his help in the *fs*-TA measurements. This project has been supported by the National Key R&D Program of China (2019YFA0906300, 2017YFA0503700, 2021YFA1300403), the Natural Science Foundation of China (NSFC, No. 22173115), the Youth Innovation Promotion Association of CAS (2020081), the CAS Interdisciplinary Innovation Team (JCTD-2020-06), the CAS Project for Young Scientists in Basic Research (YSBR-004), the CAS Key Research program for Frontier Science (QYZDY-SSW-SMC003), and the China Scholarship Council Ph.D. studentship (202006360048).

AUTHOR CONTRIBUTIONS

Conceptualization and original draft, D.-H. Li and J.-P. Zhang; Data analysis, D.-H. Li; Experiment conduction, D.-H. Li, Y. Zhang, Y.-M. Zhou, R.-Y. Gao, and H.-D. Yao; Sample preparation, C. Zhou, S. Zhao; Supervision, W. Wang, L.-M. Fu, P. Wang, and J.-P. Zhang; Project budget and MS review and editing, T. Kuang, J.-R. Shen, and J.-P. Zhang.

DECLARATIONOF INTERESTS

The authors declare no competing interests.

Received: August 15, 2022
Revised: October 10, 2022
Accepted: December 6, 2022
Published: January 20, 2023

REFERENCES

1. Peter, G.F., and Thornber, J.P. (1991). Biochemical composition and organization of higher plant photosystem II light-harvesting pigment-proteins. J. Biol. Chem. *266*, 16745–16754.

2. Ruban, A.V. (2013). The Photosynthetic Membrane: Molecular Mechanisms and Biophysics of Light Harvesting (Wiley).

3. Standfuss, J., Terwisscha van Scheltinga, A.C., Lamborghini, M., and Kühlbrandt, W. (2005). Mechanisms of photoprotection and nonphotochemical quenching in pea light-harvesting complex at 2.5 Å resolution. EMBO J. *24*, 919–928.

4. Ruban, A.V., Johnson, M.P., and Duffy, C.D.P. (2012). The photoprotective molecular switch in the photosystem II antenna. Biochim. Biophys. Acta *1817*, 167–181.

5. Ruban, A.V., Berera, R., Ilioaia, C., Van Stokkum, I.H.M., Kennis, J.T.M., Pascal, A.A., Van Amerongen, H., Robert, B., Horton, P., and Van Grondelle, R. (2007). Identification of a mechanism of photoprotective energy dissipation in higher plants. Nature *450*, 575–578.

6. Young, A., and Britton, G. (1993). Carotenoids in Photosynthesis (Springer-science+business media).

7. Latowski, D., Szymanska, R., and Strzałka, K. (2014). Carotenoids involved in antioxidant system of chloroplasts. In Oxidative Damage to Plants: Antioxidant network and signaling, P. Ahmad, ed. (Elsevier), pp. 289–319.

8. Saccon, F., Durchan, M., Kaňa, R., Prášil, O., Ruban, A.V., and Polívka, T. (2019). Spectroscopic properties of violaxanthin and lutein triplet states in LHCII are independent of carotenoid composition. J. Phys. Chem. B *123*, 9312–9320.

9. Artes Vivancos, J.M., Van Stokkum, I.H.M., Saccon, F., Hontani, Y., Kloz, M., Ruban, A., Van Grondelle, R., and Kennis, J.T.M. (2020). Unraveling the excited-state dynamics and light-harvesting functions of xanthophylls in light-harvesting complex II using femtosecond stimulated Raman spectroscopy. J. Am. Chem. Soc. *142*, 17346–17355.

10. Pascal, A.A., Liu, Z., Broess, K., Van Oort, B., Van Amerongen, H., Wang, C., Horton, P., Robert, B., Chang, W., and Ruban, A. (2005). Molecular basis of photoprotection and control of photosynthetic light-harvesting. Nature *436*, 134–137.

11. Chmeliov, J., Gelzinis, A., Songaila, E., Augulis, R., Duffy, C.D.P., Ruban, A.V., and Valkunas, L. (2016). The nature of self-regulation in photosynthetic light-harvesting antenna. Nat. Plants *2*, 16045.

12. Duffy, C.D.P., Chmeliov, J., Macernis, M., Sulskus, J., Valkunas, L., and Ruban, A.V. (2013). Modeling of fluorescence quenching by lutein in the plant light-harvesting complex LHCII. J. Phys. Chem. B *117*, 10974–10986.

13. Son, M., Pinnola, A., Gordon, S.C., Bassi, R., and Schlau-Cohen, G.S. (2020). Observation of dissipative chlorophyll-to-carotenoid energy transfer in light-harvesting complex II in membrane nanodiscs. Nat. Commun. *11*, 1295.

14. Bode, S., Quentmeier, C.C., Liao, P.N., Hafi, N., Barros, T., Wilk, L., Bittner, F., and Walla, P.J. (2009). On the regulation of photosynthesis by excitonic interactions between carotenoids and chlorophylls. Proc. Natl. Acad. Sci. USA *106*, 12311–12316.

15. Holleboom, C.P., and Walla, P.J. (2014). The back and forth of energy transfer between carotenoids and chlorophylls and its role in the regulation of light harvesting. Photosynth. Res. *119*, 215–221.

16. Van Amerongen, H., and Van Grondelle, R. (2001). Understanding the energy transfer function of LHCII, the major light-harvesting complex of green plants. J. Phys. Chem. B *105*, 604–617.

17. Cupellini, L., Calvani, D., Jacquemin, D., and Mennucci, B. (2020). Charge transfer from the carotenoid can quench chlorophyll excitation in antenna complexes of plants. Nat. Commun. *11*, 662.

18. Liu, Z., Yan, H., Wang, K., Kuang, T., Zhang, J., Gui, L., An, X., and Chang, W. (2004). Crystal structure of spinach major light-harvesting complex at 2.72 Å resolution. Nature *428*, 287–292.

19. Shen, L., Huang, Z., Chang, S., Wang, W., Wang, J., Kuang, T., et al. (2019). Structure of a $C_2S_2M_2N_2$-type PSII–LHCII supercomplex from the green alga *Chlamydomonas reinhardtii*. Proc. Natl. Acad. Sci. USA *116*, 21246–21255.

20. Wei, X., Su, X., Cao, P., Liu, X., Chang, W., Li, M., Zhang, X., and Liu, Z. (2016). Structure of spinach photosystem II-LHCII supercomplex at 3.2 Å resolution. Nature *534*, 69–74.

21. Sheng, X., Watanabe, A., Li, A., Kim, E., Song, C., Murata, K., Song, D., Minagawa, J., and Liu, Z. (2019). Structural insight into light harvesting for photosystem II in green algae. Nat. Plants *5*, 1320–1330.

22. Su, X., Ma, J., Wei, X., Cao, P., Zhu, D., Chang, W., et al. (2017). Structure and assembly mechanism of plant $C_2S_2M_2$-type PSII-LHCII supercomplex. Science *357*, 815–820.

23. Wang, W., Qin, X., Sang, M., Chen, D., Wang, K., Lin, R., Lu, C., Shen, J.R., and Kuang, T. (2013). Spectral and functional studies on siphonaxanthin-type light-harvesting complex of photosystem II from *Bryopsis corticulans*. Photosynth. Res. *117*, 267–279.

24. Akhtar, P., Nowakowski, P.J., Wang, W., Do, T.N., Zhao, S., Siligardi, G., Garab, G., Shen, J.R., Tan, H.S., and Lambrev, P.H. (2020). Spectral tuning of light-harvesting complex II in the siphonous alga *Bryopsis corticulans* and its effect on energy transfer dynamics. Biochim. Biophys. Acta. Bioenerg. *1861*, 148191.

25. Li, D.-H., Wang, W., Zhou, C., Zhang, Y., Wang, P., Shen, J.-R., Kuang, T., and Zhang, J.-P. (2020). Excitation dynamics and relaxation in the major antenna of a marine green alga *Bryopsis corticulans*. Biochim. Biophys. Acta. Bioenerg. *1861*, 148186.

26. Giovagnetti, V., Han, G., Ware, M.A., Ungerer, P., Qin, X., Wang, W.-D., Kuang, T., Shen, J.-R., and Ruban, A.V.((2018). A siphonous morphology affects light-harvesting modulation in the intertidal green macroalga *Bryopsis corticulans* (Ulvophyceae). Planta *247*, 1293–1306.

27. Polívka, T., and Sundström, V. (2004). Ultrafast dynamics of carotenoid excited states-from solution to natural and artificial systems. Chem. Rev. *104*, 2021–2071.

28. Zigmantas, D., Hiller, R.G., Sharples, F.P., Frank, H.A., Sundström, V., and Polívka, T. (2004). Effect of a conjugated carbonyl group on the photophysical properties of carotenoids. Phys. Chem. Chem. Phys. *6*, 3009–3016.

29. Seely, G.R. (1978). The energetics of electron-transfer reactions of chlorophyll and other compounds. Photochem. Photobiol. *27*, 639–654.

30. Bricker, W.P., Shenai, P.M., Ghosh, A., Liu, Z., Enriquez, M.G.M., Lambrev, P.H., Tan, H.-S., Lo, C.S., Tretiak, S., Fernandez-Alberti, S., and Zhao, Y. (2015). Non-radiative relaxation of photoexcited chlorophylls: theoretical and experimental study. Sci. Rep. *5*, 13625.

31. Niedzwiedzki, D.M., and Blankenship, R.E. (2010). Singlet and triplet excited state properties of natural chlorophylls and bacteriochlorophylls. Photosynth. Res. *106*, 227–238.

32. Saccon, F., Durchan, M., Bína, D., Duffy, C.D.P., Ruban, A.V., and Polívka, T. (2020). A protein environment-modulated energy dissipation channel in LHCII antenna complex. iScience *23*, 101430.

33. Staleva-Musto, H., Kuznetsova, V., Bína, D., Litvín, R., and Polívka, T. (2020). Intramolecular charge-transfer state of carotenoids siphonaxanthin and siphonein: function of non-conjugated acyl-oxy group. Photosynth. Res. *144*, 127–135.

34. Schulte, T., Niedzwiedzki, D.M., Birge, R.R., Hiller, R.G., Polívka, T., Hofmann, E., and Frank, H.A. (2009). Identification of a single peridinin sensing Chl-a excitation in reconstituted PCP by crystallography and spectroscopy. Proc. Natl. Acad. Sci. USA *106*, 20764–20769.

35. Kosumi, D., Kita, M., Fujii, R., Sugisaki, M., Oka, N., Takaesu, Y., Taira, T., Iha, M., and Hashimoto, H. (2012). Excitation energy-transfer dynamics of brown algal photosynthetic antennas. J. Phys. Chem. Lett. *3*, 2659–2664.

36. Akimoto, S., Yokono, M., Higuchi, M., Tomo, T., Takaichi, S., Murakami, A., and Mimuro, M. (2008). Solvent effects on excitation relaxation dynamics of a keto-carotenoid, siphonaxanthin. Photochem. Photobiol. Sci. *7*, 1206–1209.

37. Akimoto, S., Tomo, T., Naitoh, Y., Otomo, A., Murakami, A., and Mimuro, M. (2007). Identification of a new excited state responsible for the in vivo unique absorption band of siphonaxanthin in the green alga *Codium fragile*. J. Phys. Chem. B *111*, 9179–9181.

38. Akimoto, S., Yamazaki, I., Murakami, A., Takaichi, S., and Mimuro, M. (2004). Ultrafast excitation relaxation dynamics and energy transfer in the siphonaxanthin-containing green alga *Codium fragile*. Chem. Phys. Lett. *390*, 45–49.

39. Di Valentin, M., Meneghin, E., Orian, L., Polimeno, A., Büchel, C., Salvadori, E., Kay, C.W.M., and Carbonera, D. (2013). Triplet-triplet energy transfer in fucoxanthin-chlorophyll protein from diatom *Cyclotella meneghiniana*: insights into the structure of the complex. Biochim. Biophys. Acta *1827*, 1226–1234.

40. Di Valentin, M., Büchel, C., Giacometti, G.M., and Carbonera, D. (2012). Chlorophyll triplet quenching by fucoxanthin in the fucoxanthin-chlorophyll protein from the diatom *Cyclotella meneghiniana*. Biochem. Biophys. Res. Commun. *427*, 637–641.

41. Bautista, J.A., Hiller, R.G., Sharples, F.P., Gosztola, D., Wasielewski, M., and Frank, H.A. (1999). Singlet and triplet energy transfer in the peridinin - chlorophyll *a* - protein from *Amphidinium carterae*. J. Phys. Chem. A *103*, 2267–2273.

42. Neves-Petersen, M.T., Gryczynski, Z., Lakowicz, J., Fojan, P., Pedersen, S., Petersen, E., and Bjørn Petersen, S. (2002). High probability of disrupting a disulphide bridge mediated by an endogenous excited tryptophan residue. Protein Sci. *11*, 588–600.

43. Fujita, I., Davis, M.S., and Fajer, J. (1978). Anion radicals of pheophytin and chlorophyll *a*: their role in the primary charge separations of plant photosynthesis. J. Am. Chem. Soc. *100*, 6280–6282.

44. Chauvet, J.P., Viovy, R., Santus, R., and Land, E.J. (1981). One-electron oxidation of photosynthetic pigments in micelles. Bacteriochlorophyll *a*, chlorophyll *a*, chlorophyll *b*, and pheophytin *a*. J. Phys. Chem. *85*, 3449–3456.

45. Vrettos, J.S., Stewart, D.H., de Paula, J.C., and Brudvig, G.W. (1999). Low-temperature optical and resonance Raman spectra of a carotenoid cation radical in photosystem II. J. Phys. Chem. B *103*, 6403–6406.

46. Zhang, J.-P., Skibsted, L.H., Fujii, R., and Koyama, Y. (2001). Transient absorption from the $1B_u^+$ state of all-trans-β-carotene newly identified in the near-infrared region. Photochem. Photobiol. *73*, 219–222.

47. Zhang, J.P., Inaba, T., Watanabe, Y., and Koyama, Y. (2000). Excited-state dynamics among the $1B_u^+$, $1B_u^-$ and $2A_g^-$ states of all-*trans*-neurosporene as revealed by near-infrared time-resolved absorption spectroscopy. Chem. Phys. Lett. *332*, 351–358.

48. Han, R.M., Tian, Y.X., Wu, Y.S., Wang, P., Ai, X.C., Zhang, J.P., and Skibsted, L.H. (2006). Mechanism of radical cation formation from the excited states of zeaxanthin and astaxanthin in chloroform. Photochem. Photobiol. *82*, 538–546.

49. Liang, J., Tian, Y.-X., Yang, F., Zhang, J.-P., and Skibsted, L.H. (2009). Antioxidant synergism between carotenoids in membranes. Astaxanthin as a radical transfer bridge. Food Chem. X. *115*, 1437–1442.

50. Gall, A., Berera, R., Alexandre, M.T.A., Pascal, A.A., Bordes, L., Mendes-Pinto, M.M., Andrianambinintsoa, S., Stoitchkova, K.V., Marin, A., Valkunas, L., et al. (2011). Molecular adaptation of photoprotection: triplet states in light-harvesting proteins. Biophys. J. *101*, 934–942.

51. Peterman, E.J., Dukker, F.M., van Grondelle, R., and van Amerongen, H. (1995). Chlorophyll *a* and carotenoid triplet states in light-harvesting complex II of higher plants. Biophys. J. *69*, 2670–2678.

52. Kosumi, D., Horibe, T., Sugisaki, M., Cogdell, R.J., and Hashimoto, H. (2016). Photoprotection mechanism of light-harvesting antenna complex from purple bacteria. J. Phys. Chem. B *120*, 951–956.

53. Trinkunas, G., Connelly, J.P., Müller, M.G., Valkunas, L., and Holzwarth, A.R. (1997). Model for the excitation dynamics in the light-harvesting complex II from higher plants. J. Phys. Chem. B *101*, 7313–7320.

54. Van Stokkum, I.H.M., Larsen, D.S., and Van Grondelle, R. (2004). Global and target analysis of time-resolved spectra. Biochim. Biophys. Acta *1657*, 82–104.

55. Mascoli, V., Liguori, N., Cupellini, L., Elias, E., Mennucci, B., and Croce, R. (2021). Uncovering the interactions driving carotenoid binding in light-harvesting complexes. Chem. Sci. *12*, 5113–5122.

56. Son, M., Pinnola, A., Bassi, R., and Schlau-Cohen, G.S. (2019). The electronic structure of lutein 2 is optimized for light harvesting in plants. Chem *5*, 575–584.

57. Holt, N.E., Zigmantas, D., Valkunas, L., Li, X.P., Niyogi, K.K., and Fleming, G.R. (2005). Carotenoid cation formation and the regulation of photosynthetic light harvesting. Science *307*, 433–436.

58. Kiss, A.Z., Ruban, A.V., and Horton, P. (2008). The PsbS protein controls the organization of the photosystem II antenna in higher plant thylakoid membranes. J. Biol. Chem. *283*, 3972–3978.

59. Avenson, T.J., Ahn, T.K., Niyogi, K.K., Ballottari, M., Bassi, R., and Fleming, G.R. (2009). Lutein can act as a switchable charge transfer quencher in the CP26 light-harvesting complex. J. Biol. Chem. *284*, 2830–2835.

60. Liao, P.N., Holleboom, C.P., Wilk, L., Kühlbrandt, W., and Walla, P.J. (2010). Correlation of Car $S_1 \rightarrow$ Chl with Chl $\rightarrow$ Car S_1 energy transfer supports the excitonic model in quenched light harvesting complex II. J. Phys. Chem. B *114*, 15650–15655.

61. Müller, M.G., Lambrev, P., Reus, M., Wientjes, E., Croce, R., and Holzwarth, A.R. (2010). Singlet energy dissipation in the photosystem II light-harvesting complex does not involve energy transfer to carotenoids. ChemPhysChem *11*, 1289–1296.

62. Ostroumov, E.E., Götze, J.P., Reus, M., Lambrev, P.H., and Holzwarth, A.R. (2020). Characterization of fluorescent chlorophyll charge-transfer states as intermediates in the excited state quenching of light-harvesting complex II. Photosynth. Res. *144*, 171–193.

63. Parson, W.W., and Warshel, A. (1987). Spectroscopic properties of photosynthetic reaction centers. 2. Application of the theory to *Rhodopseudomonas viridis*. J. Am. Chem. Soc. *109*, 6152–6163.

64. Cupellini, L., Caprasecca, S., Guido, C.A., Müh, F., Renger, T., and Mennucci, B. (2018). Coupling to charge transfer states is the key to modulate the optical bands for efficient light harvesting in purple bacteria. J. Phys. Chem. Lett. *9*, 6892–6899.

65. Ramanan, C., Ferretti, M., van Roon, H., Novoderezhkin, V.I., and van Grondelle, R. (2017). Evidence for coherent mixing of excited and charge-transfer states in the major plant light-harvesting antenna, LHCII. Phys. Chem. Chem. Phys. *19*, 22877–22886.

66. Connolly, J.S., Samuel, E.B., and Janzen, A.F. (1982). Effects of solvent on the fluorescence properties of bacteriochlorophyll *a*. Photochem. Photobiol. *36*, 565–574.

67. Kosumi, D., Nishiguchi, T., Amao, Y., Cogdell, R.J., and Hashimoto, H. (2018). Singlet and triplet excited states dynamics of photosynthetic pigment chlorophyll *a* investigated by sub-nanosecond pump-probe spectroscopy. J. Photochem. Photobiol. Chem. *358*, 374–378.

68. Correia, R.F., Viseu, M.I., and Andrade, S.M. (2014). Aggregation/disaggregation of chlorophyll *a* in model phospholipid-detergent vesicles and micelles. Photochem. Photobiol. Sci. *13*, 907–916.

69. Van Oort, B., Maréchal, A., Ruban, A.V., Robert, B., Pascal, A.A., de Ruijter, N.C.A., van Grondelle, R., and van Amerongen, H. (2011). Different crystal morphologies lead to slightly different conformations of light-harvesting complex II as monitored by variations of the intrinsic fluorescence lifetime. Phys. Chem. Chem. Phys. *13*, 12614–12622.

70. Havaux, M., Dall'Osto, L., and Bassi, R. (2007). Zeaxanthin has enhanced antioxidant capacity with respect to all other xanthophylls in Arabidopsis leaves and functions independent of binding to PSII antennae. Plant Physiol. *145*, 1506–1520.

71. Walla, P.J., Yom, J., Krueger, B.P., and Fleming, G.R. (2000). Two-photon excitation spectrum of light-harvesting complex II and fluorescence upconversion after one-and two-photon excitation of the carotenoids. J. Phys. Chem. B *104*, 4799–4806.

72. Balevičius, V., Jr., Fox, K.F., Bricker, W.P., Jurinovich, S., Prandi, I.G., Mennucci, B., and Duffy, C.D.P. (2017). Fine control of chlorophyll-carotenoid interactions defines the functionality of light-harvesting proteins in plants. Sci. Rep. *7*, 13956.

73. Chen, H., Shen, S., Liang, Y., Leng, J., Tang, M., and Gong, Y. (2005). Evidence for dissociation of chlorophyll *b* from the main light-harvesting complex in the oligomerization state isolated from marine alga *Bryopsis corticulans*. Biochim. Biophys. Acta *1707*, 170–178.

74. Ma, F., Kimura, Y., Zhao, X.H., Wu, Y.S., Wang, P., Fu, L.M., Wang, Z.Y., and Zhang, J.P. (2008). Excitation dynamics of two spectral forms of the core complexes from photosynthetic bacterium *Thermochromatium tepidum*. Biophys. J. *95*, 3349–3357.

75. Shi, Y., Zhao, N.J., Wang, P., Fu, L.M., Yu, L.J., Zhang, J.P., and Wang-Otomo, Z.Y. (2015). Thermal adaptability of the light-harvesting complex 2 from *Thermochromatium tepidum*: temperature-dependent excitation transfer dynamics. J. Phys. Chem. B *119*, 14871–14879.

STAR★METHODS

KEY RESOURCES TABLE

REAGENT or RESOURCE	SOURCE	IDENTIFIER
Software and algorithms		
Matlab R2021b	Mathworks	https://uk.mathworks.com
Glotaran 1.5.1	Glotaran	https://glotaran.org
Origin 2021b	Origin Lab	https://www.originlab.com/

RESOURCE AVAILABILITY

Lead contact

Further information and requests for resources should be directed to and will be fulfilled by the lead contact, Jian-Ping Zhang (jpzhang@ruc.edu.cn).

Materials availability

This study did not generate new materials.

Data and code availability

- All data reported in this paper will be shared by the lead contact upon request.
- The MATLAB code for curve fitting will be shared by the lead contact upon request.
- Any additional information concerned with the data reported in this work is available from the lead contact upon reasonable request.

EXPERIMENTAL MODEL AND SUBJECT DETAILS

This study does not use experimental methods typical in the life sciences.

METHOD DETAILS

Sample preparation

The trimeric LHCIIs from *B. corticulans* and spinach were prepared following the protocols reported in ref. [23] and ref. [73], respectively. The LHCII preparations for spectroscopic measurements were solubilized in a TMK·NaOH buffer containing 50 mM Tricine (pH 7.8), 10 mM $MgCl_2$, 10 mM KCl, and 0.02% (w/v) *n*-dodecyl-α-D-maltoside (α-DDM; Sigma-Aldrich).

Absorption spectra

UV-visible absorption spectra were measured with a Cary 60 spectrophotometer (Agilent Technologies Inc., USA).

Fluorescence spectroscopies

Fluorescence spectra were recorded with an FS5 spectrofluorometer (Edinburgh Instruments, UK), for which the optical density (OD) of the LHCII samples was kept below 0.04 at the Q_y absorption maxima in order to minimize the inner filter and the self-absorption effects.

The absolute fluorescence quantum yield, Φ_{FL}, was measured with a FLS 980 fluorescence spectrometer equipped with an integration sphere (Edinburgh Instrument, UK), for which the LHCII samples were adjusted to $OD_{Qy} \approx 0.02$.

Fluorescence decay kinetics were measured by using a picosecond time-resolved fluorescence spectrometer (FLS 980, Edinburgh Instruments, UK) equipped with the time-correlated single-photon counting electronics (TCSPC). The excitation light pulses were supplied by a diode laser system (60 ps, 20 MHz), and the time resolution was about 200 ps.

Spectroelectrochemical (SEC) spectroscopy

In the SEC experiments, Chl *a* (>85%) and Chl *b* (>90%) from Sigma-Aldrich were used as received. Solvents *N, N*-dimethylformamide (DMF) and dichloromethane (DCM) were from Innochem Technology (Beijing), and were treated overnight with molecular sieves and neutral alumina before utilization.[43,44] The Chl *a* or Chl *b* solutions (1×10^{-5} M) were rigorously degassed prior to the SEC measurements. The SEC cuvette was a quartz cell with an optical path length of 1.0 mm (ALS Co. Ltd, Tokyo, Japan). The working and the counter electrodes were platinum gauze and platinum wire, respectively, while a non-aqueous Ag/Ag^{+} electrode was used as a reference (RE-7, ALS Co. Ltd., Tokyo, Japan). Working potentials were supplied by an electrochemical workstation (CHI 660E, CH Instruments Inc., China), and the spectra in 300-1000 nm were recorded on a Cary 60 spectrophotometer (Agilent Technologies Inc., USA).

Femtosecond time-resolved absorption (*fs*-TA) spectroscopy

The *fs*-TA spectrometer with a 120 fs time resolution, as determined as the full width at half maximum (FWHM) of instrumental response function (IRF), was described in detail elsewhere.[74,75] Briefly, a regenerative amplifier (SPTF-100F-1KHPR, Spectra Physics) combined with an optical parametric amplifier (OPA) provided the actinic laser at a desired wavelength with a spectral bandwidth of 10 nm (FWHM). A white-light continuum probe was generated from a sapphire plate of 3 mm thickness and, after interrogating the excited sample, was detected with a liquid-nitrogen cooled charge-coupled device (CCD; Spec-10:400B/LN, Princeton Instruments) attached to an imaging spectrograph (SpectraPro 2300i; Princeton Instruments). To minimize the possible nonlinear effects, the lowest possible excitation energy (<100 nJ/Pulse) as limited by a reasonable signal-to-noise ratio was applied to the samples. The laser source was run at a repetition rate of 100 Hz to ensure that each pulse excited the dynamically relaxed sample. The sample OD at an excitation wavelength was adjusted to 0.3–0.5 in terms of an optical path length of 1 mm. Steady-state absorption spectra were checked for the samples before and after the measurements, and no appreciable sample degradation was observed. All the measurements were carried out at room temperature (296 K).

QUANTIFICATION AND STATISTICAL ANALYSIS

For all the experiments, detail of the statistical tests used is indicated in the figure legends.